Towards an engineering-oriented strategy for building microbial anodes for microbial fuel cells

Diana Pocaznoi,* Benjamin Erable, Luc Etcheverry, Marie-Line Delia and Alain Bergel

The objective of the work was to give some first insight into an engineering-oriented approach to MFC design by focusing on anode optimisation. The effect of various parameters was firstly investigated in half cell set-ups under well-controlled conditions. Microbial anodes were formed from soil leachate under polarisation at −0.2 V *vs.* SCE with different concentrations of substrate, salt and buffer. It was shown that non-turnover CV could be used to assess the electroactive maturity of the anodes during polarisation. This first phase resulted in the definition of a set of optimal parameter values. In the second phase, an optimal anode was formed in a half-cell under the defined optimal conditions. A numerical approach was then developed to calculate the theoretical maximum power that the anode could provide in an ideal MFC. The concept of "ideal MFC" introduced here allowed the theoretical maximum power to be calculated on the sole basis of the kinetic characteristics of the anode. Finally, a MFC designed in the aim of approaching such ideal conditions generated stable power densities of 6.0 W m^{-2}, which were among the highest values reported so far. The discrepancy between the theoretical maximum (8.9 W m^{-2}) and the experimental results pointed out some limit due to the source of inoculum and suggested possible paths to improvement.

Introduction

The discovery of the capability of some microbial cells[1] and biofilms[2,3] to achieve direct electron transfer with electrodes has sparked considerable interest in the microbial fuel cell (MFC) technology. Nevertheless, after an exponential increase in the power provided by laboratory set-ups, maximum power densities have levelled off at 6.9 W m^{-2} [4] as shown in a comprehensive review dating from 2009.[5] On the basis of recent reviews[6–8] examples of the highest power densities reported in the literature are listed in Table 1. To our knowledge, no power density higher than 6.9 W m^{-2} has been reported so far. Most MFCs have provided power densities between 1 and 3 W m^{-2} (with respect to the anode surface area) either with mixed inoculum sources or pure cultures. To overcome the different scientific and technical bottlenecks[7–10] new research paths have to be explored.

Among the emerging trends, it can be observed that an increasing number of studies have turned toward separating the different MFC components and investigating them individually. Actually, complete MFC devices give complex information resulting from multiple interacting phenomena. For instance, the anode and cathode potentials can vary greatly as a function of time in a MFC, which leads to time-varying conditions during biofilm formation and increases the difficulty of data explanation. As a consequence, anodes and cathodes are more and more often investigated in half-cell set-ups under well-controlled electrochemical conditions. The anode or the cathode can thus be characterized independently leading to data that are easier to interpret. It should be acknowledged that applying a controlled potential requires rather costly electrochemical equipment, but less expensive solutions have recently been offered.[11] In this way, significant advances have been made in the fundamental understanding of microbial anodes. It has become possible to establish correlations between the applied potential and the composition of the electroactive microbial communities[12,13] and to define improved protocols for the formation of efficient[14] and reproducible[17] anodes. Well-controlled potentials have also been applied to select electroactive strains[15,16] or to form mutants with improved electroactive properties.[17] Practically, working in a half-cell has led to a jump in maximal current densities, which have recently reached 30.8 A m^{-2} [18] and up to 66 A m^{-2} under particular conditions.[19]

Breaking down a global process into its elementary components and studying each component individually constitutes the first step of the conventional engineering strategy for developing complex chemical processes. Research on MFCs

Laboratoire de Génie Chimique CNRS-Université de Toulouse (INPT), 4 allée Emile Monso BP 84234, 31234 Toulouse, France. E-mail: diana.pocaznoi@ensiacet.fr; Tel: +33 5 34 32 36 73

Table 1 Overview of microbial fuel cell performance based on the review articles[6–8] with supplements

Inoculum	J_{max}, A m^{-2}	P_{max}, W m^{-2}	Mediator	MFC type	Ref.
A previously enriched exoelectrogenic consortium	15	6.1	—	2 Chamber MFC (carbon felt cathode, substrate was a mixture of glucose and lactate, continuous mode)	7
Rice paddy field soil	16	2.3	—	Single chamber MFC (air cathode, lactate, batch mode)	49
A mixed bacterial culture collected from a MFC, originally inoculated with domestic wastewater and has been operated for about 1 year using acetate	26	6.9	—	Single chamber MFC (air cathode, acetate, batch mode; 200 mM phosphate buffer)	4
A mixed bacterial culture collected from a MFC, which was originally inoculated with domestic wastewater	9.9	2.8	—	Single chamber MFC (air-cathode, acetate, continuous mode)	39
Preacclimated bacteria from another MFC (originally inoculated with primary clarifier overflow) that had been running in fed batch mode for over 6 months	4	1.43	—	Single chamber MFC (air cathode, acetate, batch mode)	50
Geobacter sulfurreducens KN400	7.6	3.9	—	Mini-stacked MFC (graphite cloth cathode, acetate, batch mode)	15
Desulfovibrio desulfuricans	13	5.1	—	Single chamber MFC (air cathode, sulphate, batch mode)	51
Shewanella oneidensis MR-1	5.5	3.3	—	2 Chamber MFC (air cathode, lactate, continuous mode)	52
Rhodopseudomonas palustris DX-1	10	2.7	—	Single chamber MFC (air cathode, acetate, batch mode)	53
Geobacter sulfurreducens	4.6	1.9	—	Mini-stacked MFC (air cathode, acetate, continuous mode)	54

has already launched the first phase of this strategy. Then, all the individually optimised components must be put together like the different pieces of a puzzle. Numerical modelling is precious in this step as, without multiplying the number of experiments, it helps us to predict how an optimised element can affect the global process performance. In the case of MFCs, the characteristics of the anode, cathode, electrolyte(s), and membrane, if required, should ideally be determined and optimised independently first and then introduced into a numerical model to predict the global MFC performance for a given reactor configuration. At this stage, the reactor configuration can be numerically adapted to use each component to the best possible advantage. Finally, a minimum number of experiments should be achieved with a complete MFC prototype to compare the experimental and theoretical data. This comparison is always a source of rich discussion and possible further improvement of both the physical components and the theoretical model.

As detailed above, an increasing number of studies have investigated the elementary components of MFCs individually but works dealing with the experimental or theoretical reconstruction phase are still rare. Actually, reactor engineering has not yet been largely developed in the MFC domain, no doubt because experiments with laboratory cells are inexpensive and easy to multiply. Nevertheless, the emergence of efficient microbial anodes and the growing need for larger MFC prototypes will require this type of strategy to be applied sooner or later.

The objective of the present work was to give some first insight into an engineering-oriented approach for MFC design. The optimising work focused on the anode. Optimal parameters were identified for a microbial anode formed from soil leachate and fed with acetate. Soils remain a largely untapped source of MFC inoculum even though they contain a very wide microbial diversity, which might develop electroactive biofilms.[20] A few attempts have successfully exploited soils to form microbial anodes[21–24] and a recent study comparing different soils has suggested that they have promising potential.[25]

Anodes were formed in electrochemical half-cells under constant polarisation to determine the optimal value of various parameters (substrate, buffer and salt concentrations, biofilm age). The current–potential characteristics of the optimal anode were fitted numerically with a Nernst law, which was the basis of the MFC model. For this first work, a simple numerical MFC model was designed assuming that the ohmic drop could be neglected and that the cathode had ideal behaviour *i.e.* ensured a vertical current–potential curve. According to these assumptions the model gave the theoretical maximum power that the anode could provide in an ideal MFC.

Experimentally, the optimal anodes were shifted to MFC operation. The MFC was equipped with a cathode of large surface area that was oversized with respect to the anode in order to minimise the cathode limiting effect. The experimental MFC was thus as close as possible to the conditions assumed by the model and the experimental and theoretical data were compared on similar basis. The results confirmed the validity of the strategy of designing an optimal microbial anode in a half-cell under well-controlled conditions and then shifting it to MFC operating conditions. Moreover, the theoretical approach described here gave a simple tool for assessing the maximum theoretical power that a microbial anode could provide when integrated into an ideal MFC, on the sole basis of the current–potential curve recorded under half-cell conditions. The anode characteristics recorded in half-cell set-ups can be discussed in terms of maximum theoretical MFC power without any supplementary experiments.

Results and discussion

Step 1: define a set of initial standard conditions

The initial standard conditions may depend on the nature of the inoculum source. Nevertheless, general trends may be suggested according to the literature and our own experience.

Substrate concentration is of main importance, acetate 10 mM may be considered as a relevant initial value. High conductivity of the medium is essential for any electrochemical process but the addition of salts is not tolerated by common microbial consortia. In the absence of halophilic microorganisms a conductivity around 10 mS cm^{-1} seems a relevant value. Here 60 mM KCl was added into the initial soil leachate to get a conductivity of 12 mS cm^{-1}. Addition of buffer may both increase the medium conductivity[26,27] and improve the proton transport inside the biofilm.[28] Nevertheless, some preliminary experiments conducted with our inoculum indicated that our biofilms were sensitive to too-high a concentration of buffer. Adaptation of the inoculum to high buffer concentration should be an interesting path to be explored but here it was chosen not to add buffer under the initial standard conditions. Finally the potential applied during biofilm formation is certainly the most elusive parameter in the current state of the art. It has been demonstrated that low potential values can select for the most efficient electroactive strains and consequently form the most efficient anodes.[12] Nevertheless, high potential values have also been shown to increase the performance.[21–30] For this reason we suggest investigating this parameter early in the optimisation strategy.

To sum up, the initial standard conditions chosen were: room temperature, applied potential of −0.2 V *vs.* SCE, initial addition of 60 mM KCl in the leachate, no addition of buffer, successive additions of 10 mM acetate. Each parameter to be investigated was then studied using this set of standard conditions by varying only the parameter under consideration.

Step 2: define optimal applied potential and temperature

If a change in temperature is intended, temperature should be checked in priority because it generally has an important effect both on metabolic rates and on the selection of microorganisms. Here this parameter was not addressed because we targeted MFC working at room temperature.

The optimal applied potential should be determined by a series of identical experiments performed in parallel with the same inoculum sample but with different polarisation potential values or, better, with several working electrodes polarized at different potentials in the same reactor thanks to a multi-channel potentiostat. Such an experimental approach associated with the identification of the microbial communities has indicated −0.2 V *vs.* SCE as the optimal polarisation potential (to be published). These results are not discussed here and the applied potential was fixed at −0.2 V *vs.* SCE for all experiments.

Step 3: define optimal substrate concentration

Four electrochemical reactors were run simultaneously with different concentrations of sodium acetate: 10, 20, 50 and 100 mM. The current exhibited a similar initial increase for anodes fed with 10, 20 and 50 mM acetate. The first current peaks were reached after 14 to 18 days with maximum current densities of 2.5, 5 and 4.5 A m^{-2} for 10, 20 and 50 mM acetate respectively. The successive acetate additions then gave maximum current densities of 8 A m^{-2} for 10 mM acetate and around 12 A m^{-2} for 20 and 50 mM (Fig. 1A to C). In contrast, the current provided by the anode fed with 100 mM acetate increased slowly and reached a maximum of only 4 A m^{-2} after 32 days. In this case, after 75 days, the initial load of acetate had not been completely consumed (Fig. 1D).

Studies dealing with the dependence of the current on substrate concentration have generally shown that the current increases proportionally to substrate concentration at the lowest values and then tends to a maximum plateau at high values. The current is generally expected to obey a sigmoid variation with substrate concentration.[31] Using a microbial anode formed from a pure culture of *Geobacter sulfurreducens*, Marsili *et al.* found a proportional relationship with acetate concentrations up to 0.2 mM, the current then increased by only 20% when the acetate concentration was increased from 1.2 to 3 mM.[32] Similar behaviour has been observed with a wild microbial anode formed from effluents and fed with acetate at 0.5 to 20 mM. The current density increased proportionally up to around 3 mM and then tended to a plateau value at the higher concentrations.[31] Using a larger range of concentrations, from 0.5 to 35 mM, with a microbial anode formed from domestic wastewater, Sharma and Li observed an inhibiting effect by the highest concentrations of the different substrates (acetate, ethanol, and glucose):[33] the MFC gave maximal voltages in the range of 5 to 10 mM, which decreased at 20 and 35 mM.

A similar trend was observed here. The range of optimal concentration values was larger than that previously reported as no inhibiting effect was detected at a concentration of 50 mM. The substrate inhibiting effect can obviously be explained by the inhibition of metabolic enzyme catalyses. Nevertheless, other phenomena can also contribute, such as the pH of the solution, which may change in different ways depending on substrate concentration.[33] On the other hand, Aelterman *et al.* have noted that biofilms growing on electrode surfaces are subject to a duality that is rarely observed under natural conditions: the substrate concentration is the highest at the outer layers of the biofilm while the final electron acceptor (electrode) is only available at the inner layer.[29] This configuration may also contribute to the decrease in activity of the thickest biofilms, which are formed at the highest substrate concentrations.

The average Coulombic efficiencies (CE) for the first three acetate additions were 23, 17 and 15% at 10, 20 and 50 mM, respectively. The initial concentration of 100 mM led to only 6% CE. CE is controlled by the balance between the acetate that is consumed by the anode respiring bacteria and the acetate consumed by the non-electroactive bacteria present either in the biofilm or in the planktonic state. The soil leachate used here may contain many chemical compounds that can play the role of an electron acceptor, such as oxygen traces, nitrates, and sulphates, in competition with the anode, and a rich microbial flora that are able to use these electron acceptors. The presence of these alternative electron acceptors favoured the growth of non-electroactive bacteria[33,34] and explained the rather low CE obtained. Moreover, the diminution of the CE value observed here with increasing substrate concentration is commonly observed.[33] The increase in the substrate availability favoured the growth of the planktonic bacteria, mainly when electron acceptors are present in solution. In contrast, with increasing substrate availability, the biofilm

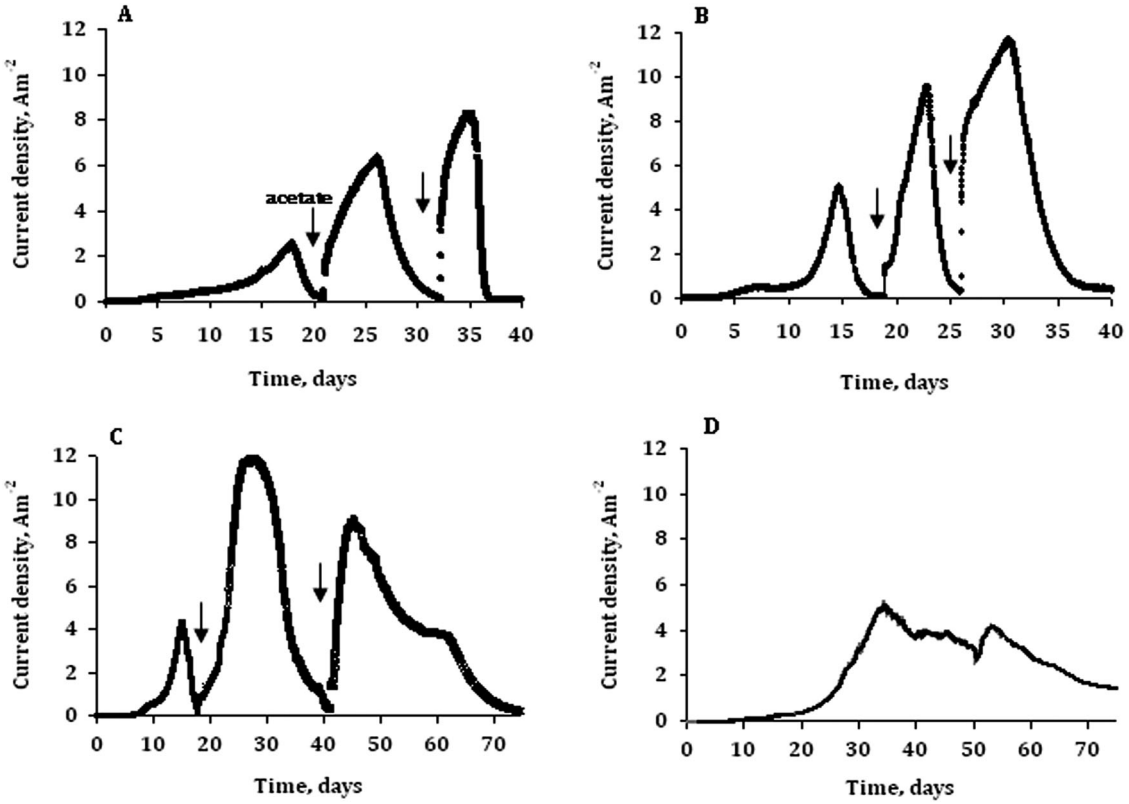

Fig. 1 Chronoamperometries of carbon cloth electrodes in soil leachate under constant polarisation at −0.2 V *vs.* SCE with successive additions of acetate at different concentrations: (A) 10 mM, (B) 20 mM, (C) 50 mM, (D) 100 mM.

development becomes limited by specific parameters, such as limited available surface area or slow mass transfer through a thick matrix. These limiting parameters unbalanced the ratio of cell growth in favour of the planktonic state at increasing substrate concentration, resulting in lower CE values.

Finally, it must be noted that the surface area of the anodes (2 cm^2) was small with respect to the bulk volume (150 mL). This configuration was drastically detrimental to CE values. In the case of a competition with homogeneous reactions, the CE value decreases for small electrode surface area. In return, the kinetics data should be of better quality because heterogeneities on the electrode surface are expected to be less marked and the maximum currents will be higher because complete depletion of the substrate occurs later. Using a small-surface-area working electrode is a basic rule in electro-analysis when the objectives are to obtain sound electrode kinetics and to reach high currents but, in this case, low CE values have to be accepted.

The pH value measured in each electrochemical reactor after a few days was around 9. A series of five experiments were carried out to observe the pH evolution in the absence of electrochemical reaction. Five reactors, each containing 150 mL compost leachate with no electrode inside, were initially supplied with 0, 10, 20, 50 and 100 mM acetate. The initial pH values were 7.0, 7.5, 8.0, 9.0 and 11.9 respectively. After 20 days all five reactors get a pH value in the range of 8.6 to 9.4, which remained stable for eight weeks. It was concluded that the alkalinization was not linked to the electrochemical reactions but was due to the spontaneous evolution of the non-buffered compost leachate.

About reproducibility

The maximum current densities depended partly on the initial bag of compost that was used to prepare the leachate. In three different experiments performed under standard conditions with different leachates, the current peaks at the third acetate addition varied from 6.3 to 8 A m^{-2}. In five different experiments performed under standard conditions but with additions of 20 mM acetate, the third current peaks varied from 12 to 16.3 A m^{-2}. In this last case, using a large volume of leachate (600 mL) to increase the amount of available acetate, with a small anode surface area (1 cm^2) to lower the acetate consumption, allowed a maximum current to be maintained for a week in the range of 13.0 to 14.5 A m^{-2}. To sum up, a total of eight experiments performed under standard conditions showed that the maximal current density may differ from one experiment to another essentially because of variability of the soils. Nevertheless, the orders of magnitude were always similar and with the same ranking.

Step 4: assess optimal biofilm electroactive maturity

During the chronoamperometry experiments, the polarisation was interrupted and cyclic voltammetry (CV) curves were recorded at 1 mV s^{-1} when the electrode provided maximum current (day 35, 31, 29 and 32, respectively, for 10, 20, 50 and 100 mM acetate; Fig. 2). CV curves exhibited a sigmoid shape with a superimposed redox event at the beginning of the plateau. The superimposed peak cannot be attributed to a transient phenomenon as it is commonly observed on CVs

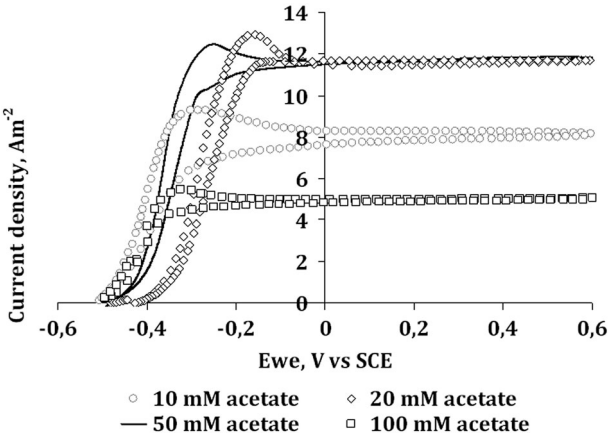

Fig. 2 Catalytic cyclic voltammetry (CV) curves (1 mV s^{-1}) recorded with the microbial anodes from Fig. 1 when currents were around maximum values.

recorded at high scan rate. In contrast, the CVs performed here at 1 mV s^{-1} can be considered as a succession of stationary states. To confirm this it can be remarked that the current densities measured on the CV curves at −0.2 V *vs*. SCE were equal to the current densities recorded during polarisation just before the interruption. Similar shapes have already been reported in the literature on CVs recorded at low scan rate[35] and a numerical approach has recently been proposed for modelling such CV curves.[36] The model is based on 5 successive steps (Fig. 3).

Step 1: mass transport of acetate, carbon dioxide and protons into and out of the biofilm (Fick's diffusion),

Step 2: microbial oxidation of acetate to carbon dioxide and protons (Michaelis-like reaction),

Step 3: electron transfer from inside the cell to the redox mediator or to the extracellular electron transfer system (irreversible first-order reaction),

Step 4: electron transport in the biofilm matrix towards the electrode surface (diffusion-like),

Step 5: electron transfer onto the anode surface (electrochemical kinetics).

The numerical CV curve exhibited a superimposed oxidation peak, similarly to the curves obtained here (Fig. 2A), only when Step 3 was rate-limiting. According to this numerical approach, it can be concluded that current production was limited here by Step 3, *i.e*. by electron transfer from the microbial cell to the electron transfer network of the biofilm (redox mediator, or conductive pili, or extracellular cytochrome…). The peak was smaller on the CV recorded with 100 mM acetate. In this case, the cell metabolism (Step 2) was inhibited by the high acetate concentration and consequently Step 3 had a lower limiting effect.

CVs were also recorded after acetate depletion at the end of the first and second current peaks (Fig. 3A–C). So-called non-turnover CVs detect the redox compounds contained in the biofilm.[37] Obviously it cannot be ascertained that the redox systems detected under non-turnover conditions are involved (or not) in acetate oxidation, nevertheless these CVs give some clear information on the redox capability of the biofilms.

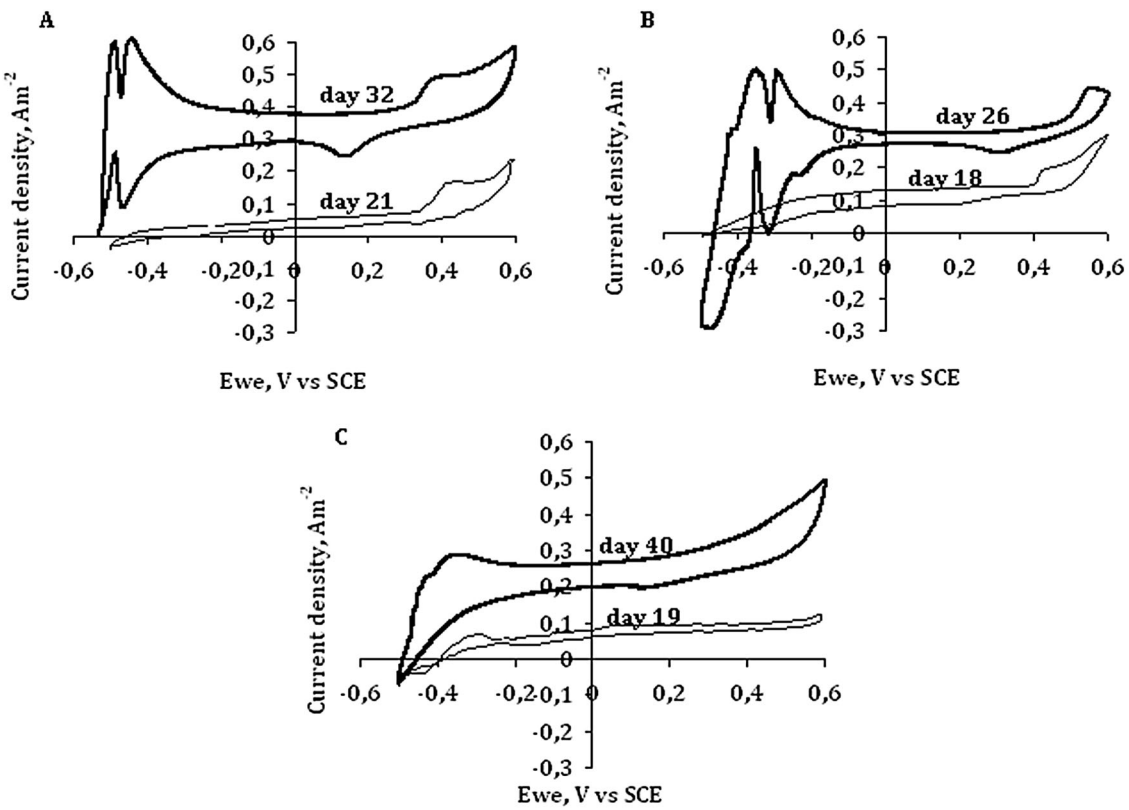

Fig. 3 Non-turnover cyclic voltammetry curves (1 mV s^{-1}) recorded with the microbial anodes from Fig. 1 when acetate was depleted after the first and the second addition of acetate (A) 10 mM, (B) 20 mM, (C) 50 mM.

The CV curves reported in Fig 3 showed that traces of acetate remained present in the solution. Low catalytic currents were observed, which shifted the curves towards positive currents. Actually, waiting for complete depletion of acetate may, in some cases, hinder the recovery of the current at the next acetate addition. For this reason it was avoided to wait too long when the current dropped down during polarisation before recording the non-turnover CV. The CV curves detected almost no redox properties inside the biofilms after the first acetate addition. In contrast, complex redox events in the potential range from −0.2 to −0.5 V *vs.* SCE appeared at the end of the second acetate addition, which indicated multiple redox properties of the biofilm. It would not make sense to extract detailed conclusions from a comparison of CVs performed on different electrodes under different operating conditions, but it is worth noting that the CV curves recorded here after the second acetate addition had a general shape close to the CV reported for electroactive biofilms formed from pure cultures of *Geobacter sulfurreducens*.[37,38] In each case, the non-turnover CVs showed that only one acetate addition was not enough to fully develop the electroactive properties of biofilms. Moreover the biofilm obtained at 50 mM showed less rich redox contents.

To conclude on this section, the concentration of 20 mM was considered as optimal here because it led to similar current density and Coulombic efficiency to 50 mM but the current peaks were shorter in time, allowing more numerous successive experiments to be done in the same period of time. Moreover, non-turnover CVs showed richer redox electron transfer capabilities for the biofilms formed with 20 mM acetate.

It should also be kept in mind that non-turnover CVs gave interesting information on the electroactive maturity of biofilms. Here, non-turnover CV proved to be a useful tool for assessing the electroactive maturity of biofilms. It seems advisable to wait until a biofilm has fully developed its electroactive capability before shifting it to MFC operation. In this way biofilms can be considered ready to be shifted to MFC operation when non-turnover CV curves show numerous current peaks in the region of low potentials. Here, two successive additions of acetate were required to reach electroactive maturity.

Step 5: effect of buffer addition

Torres *et al*. have observed a great increase in the current provided by microbial anodes in the presence of high concentration of buffer solution. They recorded current densities going from 2.2 A m^{-2} with 12.5 mM phosphate buffer to 9.3 A m^{-2} with 100 mM phosphate buffer.[28] They have shown that the current was limited by the proton transport out of the biofilm. Accumulation of the protons produced by the microbial oxidation of the substrate caused local acidification in the biofilm, which inhibited the microbial metabolisms. The authors explained that the buffering species enhanced proton transport out of the biofilm and thus limited local acidification.

To look for a possible similar effect on our microbial anodes, experiments were carried out with bicarbonate buffer, pH 9.0. Bicarbonate was chosen instead of phosphate because the pH value in the electrochemical reactors was around 9. Using a buffer with a slightly higher pK_a ensures a buffering effect that stabilises the pH.[39] Moreover, the small bicarbonate ions can transfer protons more efficiently than phosphate ions.[39] The proton transfer rate *via* monobasic phosphate has been reported to be 34% lower than that of bicarbonate because of the lower mass transfer coefficient of phosphate in water (1.0×10^{-5} cm^2 s^{-1} *vs.* 1.34×10^{-5} cm^2 s^{-1} at 30 °C).[27–39]

A microbial anode was formed under standard conditions, with three successive additions of 10 mM acetate. From day 55, the current was stabilized for six days in the range of 6.5 to 9.5 A m^{-2} by adding acetate as soon as the current began to decrease. During the stable current phase, a solution of bicarbonate buffer, pH 9.0, was added into the reactor at increasing final concentrations. Concentrations of 2.5 and 25 mM did not affect the current. Bicarbonate 50 mM immediately increased the current density by 0.8 A m^{-2} (10%), while 100 mM and 200 mM decreased the current, also immediately after addition, by 0.8 and 0.7 A m^{-2}, respectively.

The addition of 50 mM bicarbonate increased the conductivity of the medium from 12 mS cm^{-1} to 15 mS cm^{-1}. The corresponding resistivities were $\rho = 0.83$ and 0.67 Ωm. Taking into account the current density of around 7 A m^{-2}, the 2 cm^2 anode surface area and the 0.5 cm distance between the anode and the reference electrode gave ohmic drops of 29 and 23 mV without and with 50 mM carbonate, respectively. The 10% increase observed with 50 mM bicarbonate was consequently not explained by a diminution of the ohmic drop but must correspond to a slight enhancement of the proton transport inside the biofilm as observed by Torres *et al*.[28] Nevertheless, the effect was very much lower than that previously reported. Actually, the previous studies formed the biofilm in the presence of 100 mM buffer and then decreased the buffer concentration to detect its effect. It cannot be ruled out that a biofilm formed in the presence of high buffer concentration may then need the presence of buffer, for example because of the selection of particular microbial species or because the absence of buffer may destabilize its extracellular matrix. The different behaviour observed here can consequently be explained by drastic difference in operating conditions.

Besides, the low effect of the addition of buffer observed here also confirmed that diffusion was not a rate-limiting step, as indicated by the analysis of the CV curves (“Step 4: assess optimal biofilm maturation” section). This conclusion was also consistent with epifluorescent imaging of microbial anodes obtained after 7 weeks under polarisation and MFC operation, which showed biofilms essentially formed around the 8 μm diameter fibres that composed the woven structure of the cloth electrode. The biofilms sometimes formed a very thin film between the fibres but the biofilm structure remained everywhere largely opened. The biofilm structure was thus characterized by a low thickness and a large surface area exposed to the solution, which favoured mass transfer (Fig. 5). The analysis of non-turnover CV, the low effect of buffer additions and the biofilm imaging consistently indicated that mass transfer was not rate-limiting in the biofilms formed here.

To conclude, it should be noted that the effect of buffer is complex because it affects both the conductivity of the electrolyte and the proton transport inside biofilms. According to the present results, low buffer concentrations can be expected to increase the current by improving proton transport and the

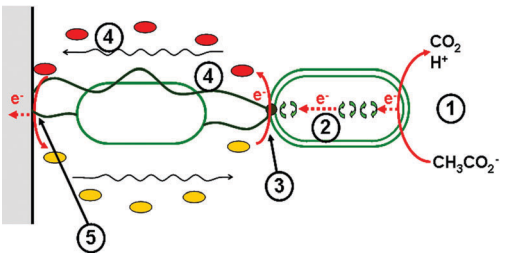

Fig. 4 Schematic representation of the electron transfer mechanism in electroactive biofilms (adapted from ref. 36): (1) diffusion of the substrate to and of the products from the microbial cell; (2) metabolic redox reactions inside the cell; (3) electron transfer from the microbial cell to the first extracellular redox compound; (4) electron transport through the electron transport network of the biofilm (diffusion of redox compounds, pili conduction…); (5) electrochemical electron transfer to the electrode surface.

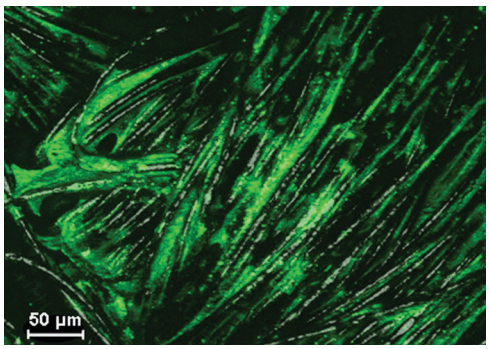

Fig. 5 Epifluorescence microscopy of the microbial anode formed on carbon cloth after 7 weeks under polarisation at −0.2 V *vs.* SCE and in MFC operation.

highest concentrations can decrease the current because of metabolic inhibition. Nevertheless, the effect of buffer can be very different depending on whether it is present or not during biofilm formation.

Step 6: effect of ionic strength

High conductivity of the electrolyte is beneficial to any large-scale electrochemical process in order to decrease the internal resistance of the reactors. To assess the capability of our anode to accept high ionic strengths, two experiments were carried out under standard conditions, with leachate that initially contained 60 mM KCl. After the fourth acetate addition, potassium chloride was added into the reactor when the current was maximum (day 42). The first 50 mM KCl addition decreased the current from 7 to 4.5 A m^{-2} after only one hour, the second 50 mM addition decreased the current to 4 A m^{-2} in one hour more. The second experiment confirmed the negative effect of KCl additions. Unfortunately, the microbial anode did not accept an increase in the ionic strength. The sensitivity to salinity revealed here can also explain the negative effect of bicarbonate above 50 mM detected in "Step 5".

It has already been pointed out that the optimum ionic strength should be found for each inoculum[40] because an excessively high ionic strength alters the osmotic pressure of the bacterial cell membrane.[41] Nevertheless, the detrimental effect of high ionic strength has rarely been demonstrated experimentally because most reported experiments have been carried out in MFC devices. In this case, increasing the ionic conductivity has two antagonistic effects: a positive effect by decreasing the internal resistance[27,42,43] and, above a threshold value, a negative effect on the microbial metabolism. It is consequently difficult to identify in MFC configuration the real value of the threshold that starts to alter the microbial metabolisms because it can be in a large extend masked by the decrease in the reactor internal resistance. In contrast, a three-electrode system minimises the ohmic drop effect (as calculated in "Step 5"). If the half-cell set-up is suitably designed, with the tip of the reference electrode as close as possible to the working electrode, the conductivity of the medium will have no significant effect on the current produced by the anode. In consequence, under polarisation in a half-cell set-up, the progressive increase in the salt concentration should not affect the current at first. The current decrease should be observed as soon as inhibition of the metabolic processes occurs. The optimal salt concentration will be the highest value that does not affect the current. Here, no KCl addition was needed in addition to the initial 60 mM concentration.

Step 7: forming microbial anodes under optimal conditions in three-electrode set-up and checking in MFC configuration

Three microbial anodes were formed in parallel under the optimal conditions defined above: polarisation at −0.2 V *vs.* SCE, additions of 20 mM acetate in three separate MFC reactors, only 60 mM KCl in the initial leachate, no addition of buffer. Three successive additions of acetate were made in two reactors (duplicates) to obtain mature electroactive biofilms according to Step 4. The current varied in the same way for the two reactors (Fig. 6). After 32 days, the polarisation was stopped and the two anodes were transferred into a MFC device. 20 mM Acetate was added when the cell tensions dropped down. The tension *vs.* time (Fig. 7) behaviour of each MFC was similar. The MFCs provided maximum power densities of 6.0 and 5.8 W m^{-2} for several days. The stationary power densities obtained were similar to the highest performance reported in the literature (Table 1). Consistently with the experiments reported in Step 5 in half-cell set-up, adding

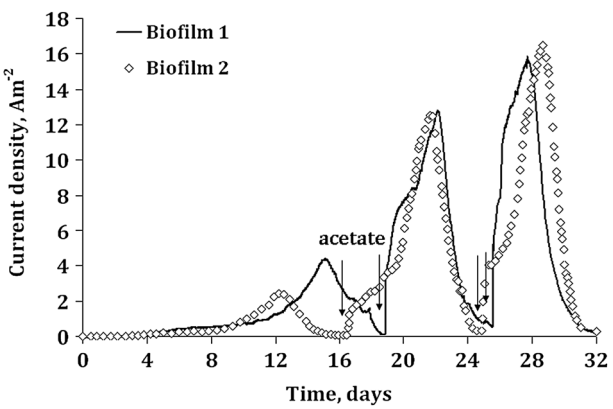

Fig. 6 Chronoamperometries of carbon cloth electrodes in soil leachate under constant polarisation at −0.2 V *vs.* SCE with three successive additions of acetate 20 mM.

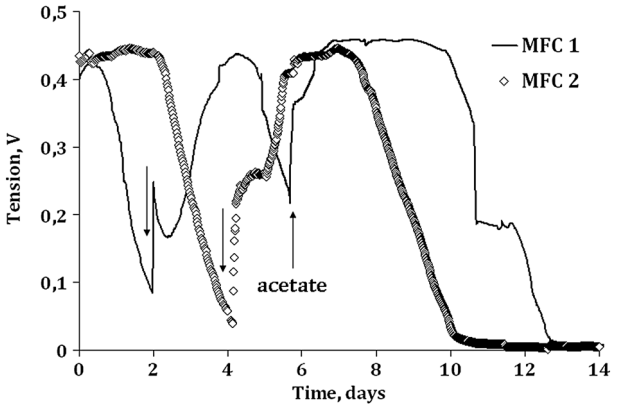

Fig. 7 Cell tension supplied by the microbial fuel cells with a 330 Ω electrical resistance. The MFCs were designed with the microbial anodes developed under chronoamperometry (Fig. 6).

50 mM bicarbonate buffer into the MFC (day 8) increased the power density from 6.0 to 6.6 W m^{-2} (10%).

The effect of the biofilm age was assessed with the third biofilm that underwent only one addition of acetate 20 mM during formation in the half-cell set-up. When shifted to MFC operation it showed some difficulty in starting with erratic behaviour, including polarisation inversion. After 11 days the stationary power poorly stabilized but never exceeded 5.6 W m^{-2} at the maximum. This result confirmed the advisability of forming electroactive mature biofilms under polarisation before operating them in MFC. Too-young biofilms have already been shown to lead to deficiency, which can be detected on the polarisation curves.[44,45] The non-turnover CV showed here to be a powerful tool for deciding whether an anode prepared under polarisation is ready to be shifted to MFC operation or requires more polarisation time. The criterion for deciding on the readiness of the biofilm should be the presence of numerous current peaks in the region of low potentials, which characterize a mature electron transport system (Fig. 4).

Polarisation curves were recorded on the two MFCs (duplicates) built with the mature biofilms at the beginning (day 0) and at days 5 and 8 of MFC operation (Fig. 8A and B). The polarisation curves gave maximum power densities of the same order of magnitude as the stationary values, with around 16% overestimation (7.0 and 6.7 W m^{-2} on the polarisation curves instead of 6.0 and 5.8 W m^{-2} at steady state). The large overshoots that have sometimes been reported in the literature were not observed here. Thanks to the reference electrode set in the MFCs, current–potential characteristics were plotted simultaneously to the polarisation curves (Fig. 8C). The anodes exhibited kinetics similar to those recorded by CV in the half-cell set-up, which confirmed that both the CV scan rate and the rate of change of the resistance values were slow enough to assess the steady state anode kinetics.

The power–current curves were not symmetrical. The maximal powers were obtained with a resistance value of 330 Ω, for which the anodes were at a potential around −0.35 V *vs.* SCE. When the electrical resistance was changed to values lower than 330 Ω, the anode provided a constant current value, which was the maximum value of around 1.5 mA. In the second branch of the polarisation curve, *i.e.* for electrical resistances lower than 330 Ω, the current was consequently constant whatever the value of the resistance. The power was limited by the anode, which was not able to provide current higher than the maximum plateau. Under such conditions, the second branch of the polarisation curve should be strictly vertical. Actually, it was slightly tilted to the right because the current decreased slightly when the potential of the anode increased. This small decrease in anodic current may have been due to a slight inhibition of the anode at high potential values.

Step 8: numerical model of an "ideal MFC"

As noted in the Introduction section, more and more studies are using polarisation in half-cells with promising results. Nevertheless, the microbial anodes formed in half-cell set-ups have rarely been checked under MFC conditions. It will consequently be of great interest to be able to predict the power that a microbial anode could provide in a MFC on the basis of the half-cell data only, without needing to repeat in a MFC the experiments already done in the half-cell.

The power density (P, W m^{-2}) provided by a fuel cell is:

$$P = (E_A - E_C)\, j - (\Sigma R\, I)j \qquad (1)$$

where E_A and E_C are the anode and cathode potentials (V), j is the current density (A m^{-2}), I is the current (A) and ΣR is the sum of resistances of electrolyte(s) and separator between the anode and the cathode (Ω). It must be noted that the terms $E_A - E_B$ are not the MFC potential difference but are calculated with the anode and cathode potentials that are measured independently under half-cell conditions.

In the aim to exploit a microbial anode optimally in an "ideal MFC", the solution resistance must be decreased, by adding salts or buffer for example, and the cathode kinetics must be faster than the anode kinetics. A practical way to overcome the cathode kinetics limit is to use a larger surface area for the cathode than the anode. Such a method has, for example, been successfully used to obtain the best MFC performance reported so far with an air-cathode,[4] with a ratio of 14 between anode and cathode surface areas. Here the MFC was designed with a ratio of 19. In an ideal MFC, the cathode would exhibit a vertical current–potential curve, meaning that the cathode potential would always keep its open circuit value ($E_{C,oc}$) whatever the current provided. Assuming such an ideal cathode and neglecting the ohmic drop (ΣR), eqn (1) gives the theoretical power density that can be provided by a microbial anode under optimal conditions:

$$P = (E_A - E_{C,oc})j \qquad (2)$$

The Nernst–Michaelis equation established by Torres *et al.* can be used to model the j–E curve of the anode:[46]

$$j = j_{max}\{1/(1 + \exp[-F/RT(E_A - E_{A,K})])\} \qquad (3)$$

where j_{max} is the maximum current density provided at the plateau, F the Faraday constant (96 485 Coulomb per mol e^-), R the gas constant (8.3145 J mol^{-1} K), T the temperature (293.15 K), and $E_{A,K}$ the anode potential at which $j = j_{max}/2$. Fitting the current–potential curve with eqn (3) showed that the anode obeyed a Nernst–Michaelis kinetics perfectly, with

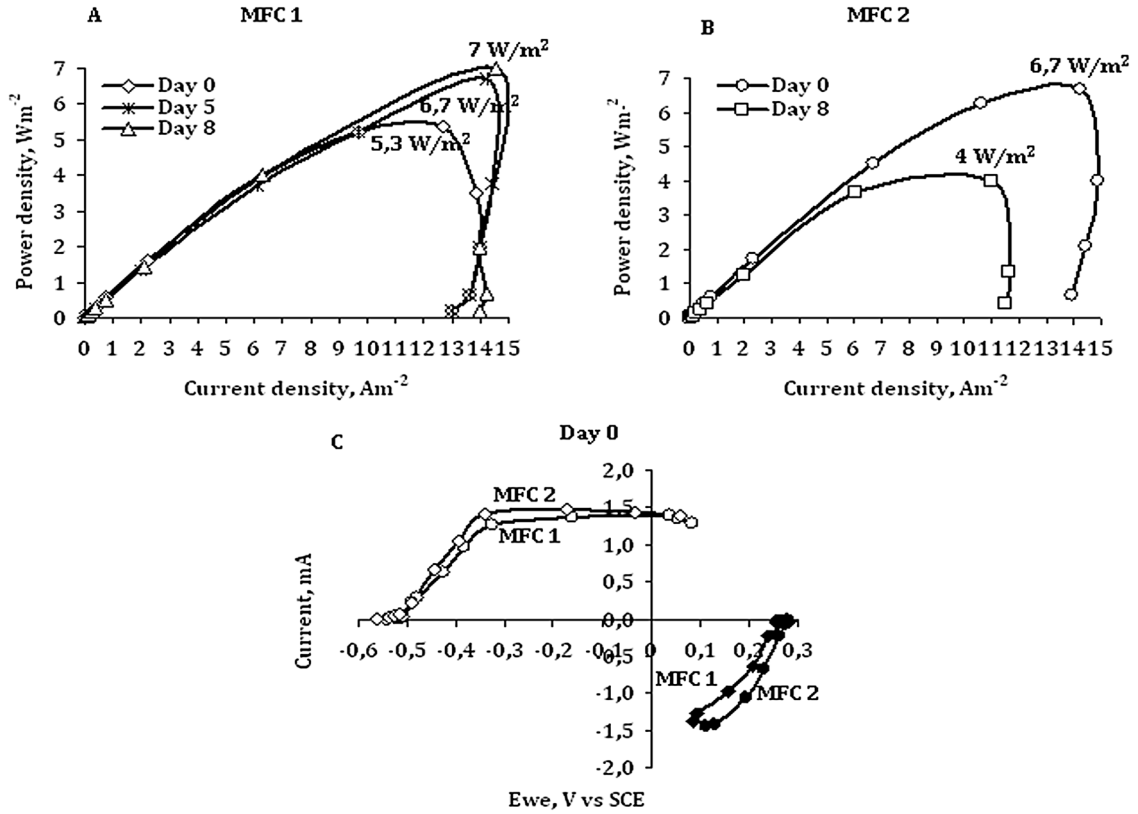

Fig. 8 MFCs electrochemical characterisation. (A) and (B) Power curves recorded at different times on the two MFCs, (C) potential–current curves.

the values $j_{max} = 14.9$ A m^{-2} and $E_{A,K} = -0.43$ V *vs.* SCE (Fig. 9A). The current–potential curve was fitted here by a Nernst–Michaelis law, for other curve shapes a Butler–Volmer-based approach may be developed.[31]

The expression of E_A extracted from eqn (3) allows the power density to be expressed as a function of the current density:

$$P = \{(E_{C,oc} - E_{A,K}) + RT/F \ln(j_{max}/j - 1)\}j \quad (4)$$

eqn (4) represents the optimal polarisation curve (P–j) that could be obtained with an ideal cathode and with no ohmic drop.

Introducing the value $E_{C,oc} = +0.28$ V *vs.* SCE, measured for the air-cathode used here, gave the polarisation curve, plotted in Fig. 9B. This polarisation curve would be reached if the MFC device ensured ideal conditions. The numerical approach confirmed that a vertical decrease in the second branch of the polarisation curve (electrical resistances lower than optimal) must be observed when the power supplied is strictly limited by the anode kinetics. A Nernst–Michaelis type anode implemented in a MFC with a large cathode surface area logically leads to such a severe dissymmetry. This dissymmetry is not a sign of a dysfunction but evidences the current limit imposed by only one electrode (it should be noted that the same dissymmetry would be obtained if the cathode alone limited the current). The model confirmed that the power maximum was determined here by the kinetically limiting anode.

Finally, eqn (4) was derived:

$$dP/dj = (E_{C,oc} - E_{A,K}) + RT/F\{\ln(j_{max}/j - 1) - j_{max}/(j_{max} - j)\} \quad (5)$$

and setting the derivative to zero:

$$(E_{C,oc} - E_{A,K}) + RT/F\{\ln(j_{max}/j - 1) - j_{max}/(j_{max} - j)\} = 0 \quad (6)$$

gives the maximum point of the polarisation curve. Eqn (6) can be solved by numerical iterations but it is more accurate to treat it as a function of E_A rather than j because, at the maximum point, the value of j is close to j_{max}, which may introduce instability in the iterative process. Eqn (6) was consequently transformed to:

$$E_A^{opt} = E_{A,K} + RT/F \ln [F/RT(E_{C,oc} - E_A^{opt})] \quad (7)$$

Solving eqn (7) by iterations gives the value of the anode potential (E_A^{opt}) at which the MFC provides the maximum power. Then, combining eqn (2) and (3) leads to the value of the theoretical maximum power density (P_{max}):

$$P_{max} = (E_A^{opt} - E_{C,oc})1/\{1 + \exp[-F/RT(E_A^{opt} - E_{A,K})]\} \quad (8)$$

In conclusion, eqn (7) and (8) give a fast assessment of the theoretical maximum power density that a microbial anode can provide on the sole basis of its current–potential curve. This curve can be recorded in a half-cell set-up and the P_{max} evaluation does not need any supplementary experiment in MFC configuration. The parameters $E_{A,K}$ and j_{max} can be easily measured from the current–potential curve. The value of the cathode potential at open circuit $E_{C,oc}$ can be extracted from the literature or measured experimentally. It is then

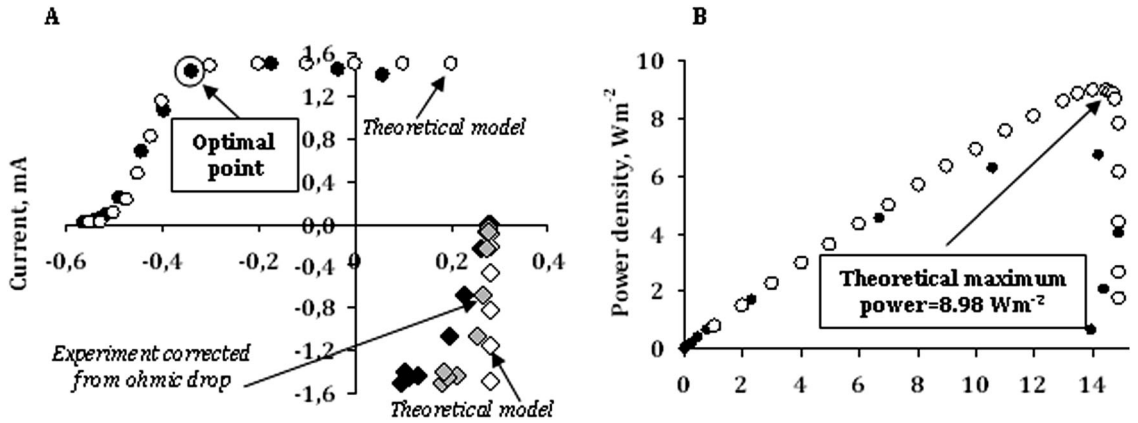

Fig. 9 Comparison of the numerical model with the experimental data obtained from MFC 2 at day 0. White (A) current–potential curves of the anode and the cathode, (B) polarization curve of the MFC. In each figure white marks represent the model and black marks the experimental data. For the cathode the grey marks represent the experimental measures corrected from the ohmic drop.

sufficient to solve eqn (7) by a simple iteration process and to put the E_A^{opt} value found into eqn (8) to get the maximum power that can be produced by the microbial anode.

Step 9: comparison of theoretical and experimental results

With the experimental data obtained here, eqn (7) gave the optimal anode potential $E_A^{opt} = -0.34$ V *vs.* SCE. This theoretical value was equal to the experimental potential that the anode had with the external resistance of 330 Ω. Eqn (8) indicated that the microbial anodes should be able to provide a maximum power density of 8.98 W m^{-2} under ideal conditions. The maximum power density of 6.7 W m^{-2} measured on the experimental curve was 25% lower than the theoretical maximum value. It is easy to observe (Fig. 9A) that, despite its large surface area, the cathode was far from the ideal verticality. Actually, both the anode and cathode potentials were measured with respect to the same reference electrode, which was close to the anode surface. The current–potential curves of the cathode consequently included the total ohmic drop of the cell. With a solution conductivity of 12 mS cm^{-1}, *i.e.* a resistivity $\rho = 0.83$ Ωm, the anode and cathode surface areas (A) of 1 and 19 cm^2 respectively, and a distance $L = 3$ cm between the two electrodes, the resistance of the solution (R_{sol}) can be calculated by:

$$R_{sol} = \rho \int_0^L dl/A \qquad (9)$$

which gives, for two disk electrodes centred on the same axis:

$$R_{sol} = \rho L/\pi\,(r_C - r_A)(1/r_A - 1/r_C) = \rho\, L/\pi r_C r_A = 57\ \Omega \qquad (10)$$

where $r_A = 0.564$ cm and $r_C = 2.46$ cm are the anode and cathode radii (the anode was assimilated to a disk for the sake of simplicity). The value of the resistance of the solution allowed the current–potential curve of the anode to be corrected from the ohmic drop:

$$E_{C,correct} = E_C + R_{sol} I \qquad (11)$$

where $E_{C,correct}$ and E_C are the corrected and the raw measured potentials (V) of the cathode and I is the current (A). At the optimal point, the measured cathode potential was +0.130 V *vs.* SCE and the corrected value $E_{C,corr} = 0.210$ V *vs.* SCE (Fig. 9A). Considering the open circuit value $E_{C,oc} = +0.28$ V *vs.* SCE indicated that the potential loss due to the cathode kinetics was 70 mV at the optimal point. On the other side, the anode with an open circuit potential $E_{A,oc} = -0.54$ V *vs.* SCE introduced a potential loss of 200 mV at the optimal point. Obviously, the potential loss due to the anode then increased drastically on the course of the second branch of the polarisation curve ($R < 330$ Ω). It reached 640 mV for the short-circuited MFC, where both anode and cathode had the same potential of +0.1 V *vs.* SCE. These values confirmed that the anode imposed the main kinetic limit, as targeted by the cell design. The cell design based on large oversizing of the cathode surface area did not fully manage to overcome the slow kinetics of the air-cathode and to exploit the anode under absolutely optimal conditions. The potential losses due to solution resistance and cathode kinetics remained significant at the optimal point and were responsible for diminishing the experimental maximum power by 25% with respect to the theoretical maximum.

The soil used here revealed a promising ability to form microbial anodes, which gave power density among the highest values reported so far. Nevertheless, comparing the experimental result with the theoretical limit revealed some bottlenecks that should be addressed in order to better exploit this source of inoculum.

The sensitivity of the microbial anodes to the addition of KCl and the poor improvement afforded by buffer addition were revealed by the experiments performed under applied potential and were confirmed in MFC operation. It would consequently be difficult to decrease the ohmic drop in a large-scale MFC. A possible path in this direction would be to try to adapt the microbial community to higher salinity as has been successfully achieved with pure culture of *Geobacter* species for instance.[47]

In spite of its large surface area, 95 mV of the potential lost was due to the cathode. At the optimal point of the power the cathode provided around 1.4 mA, *i.e.* a current density

of 0.74 A m^{-2} with respect to its surface area. The air-cathode including platinum particles used here should ensure higher current densities. Here the soil leachate was a solution highly loaded with mineral and organic matter, which induced significant (bio)fouling on the internal cathode surface. This fouling was evidenced by simple visual examination of the cathode after disassembly of the cell. Because it hampered the ionic transport to the catalyst particles, fouling was a major cause of the poor performance of the cathode.[48] This would be a serious drawback in the development of large-scale devices with this medium. To take advantage of the promising properties of the inoculum this bottleneck must be solved. Work is now turning to the use of synthetic media to decrease the organic load of the solution with the main goal of decreasing cathode fouling while keeping the anode performance.

Experimental

Formation and test of microbial anodes in three-electrode set-ups

The source of inoculum was garden compost for biological cultivation (Eco-Terre). 1 L of soil was mixed with 1.5 L of distilled water that contained 60 mM of potassium chloride. The mixture was stirred for 24 hours and then centrifuged to obtain a leachate. This soil leachate was used directly in the electrochemical reactors, only sodium acetate at different concentrations was added as substrate.

Experiments were performed using three-electrode systems (half-cells), each consisting of a 2 cm^2 carbon cloth anode (PaxiTech SAS, France), a saturated calomel reference electrode (SCE, Radiometer Analytical, potential + 0.241 V/SHE) and a 5 cm^2 platinum grid as the auxiliary electrode (Heraeus) in electrochemical reactors that contained 150 mL of soil leachate. The anode was connected to the electrical circuit with a 12 cm-long, 1 mm-diameter platinum wire. Biofilms were formed under constant polarisation at −0.2 V *vs.* SCE using a multi-channel potentiostat (VMP Biologic SA) recording the current every 1800 s. When indicated, additions of acetate were made when the current dropped to near zero. All experiments were carried out at room temperature (20 ± 2 °C) and pH was monitored during the study. The Coulombic efficiency was calculated as the ratio of the charge (Coulomb) obtained by integrating current over time, to the theoretical charge that can be produced from acetate (8 moles of electrons per mole of acetate).

Formation and use of microbial anodes in MFC

The MFC consisted of a single polypropylene chamber of 75 mL volume equipped with a 1 cm^2 carbon cloth anode and a circular 19 cm^2 air-cathode containing 1.5 mg cm^{-2} of a platinum catalyst (PaxiTech SAS, France). The anode was reduced to 1 cm^2 instead of 2 cm^2 in the 150 mL electrochemical reactors in order to keep the same surface area/volume ratio in both devices. The cathode was oversized with respect to the anode (factor of 19 between the projected surface areas) with the objective of overcoming a possible kinetic limit from the cathode and to make the anode rate-limiting. The air-cathode was exposed to air on one side of the MFC and connected to the electrical circuit through a stainless steel electrical collector placed against the side exposed to air. The microbial anode was formed under polarisation as described above for 31 days and was then transferred into the MFC chamber. The anode was connected to the air-cathode through a 330 Ω electrical resistance. Three MFCs, each containing 75 mL of the same soil leachate, were operated in parallel at room temperature. Current density *vs.* power density curves were recorded from time to time by varying the external resistance from 1 Ω to 330 kΩ every 10 minutes. A SCE reference electrode close to the anode surface allowed the potentials of the anode and cathode to be measured during recording of the polarisation curves.

Microscopy and image analysis

Microbial colonization on the anode surfaces was examined by epifluorescence microscopy. The biofilms were stained with 0.01% acridine orange (A6014, Sigma) for 10 minutes and then washed carefully with distilled water. The samples were then left to dry in ambient air and imaged using a Zeiss Axio Imager-M2 microscope.

Conclusions

This work proposed a systematic strategy for forming microbial anodes for MFCs. The first steps consisted of investigating the effect of each parameter individually under polarisation in half-cell set-ups. An optimal anode was then formed under applied potential in the half-cell with the set of defined optimal parameter values. The simple numerical approach described here permits an assessment of the theoretical maximum that the microbial anode is able to provide in MFC operation, without any experiments in MFC configuration. It thus becomes possible to discuss the results of an anode obtained in a half-cell in terms of power that could be provided in an ideal MFC.

A MFC designed with the aim of approaching the ideal conditions succeeded in providing 75% of the maximum theoretical power. Analysis of the discrepancy between the experimental results and the theoretical maximum evidenced some limits of the inoculum source that was used and mapped out some paths for future improvements.

Acknowledgements

This work was part of the "Agri-Elec (ANR-08-BioE-001)" project supported by the Bio-Energies programme of the French research agency ANR.

Notes and references

1 B. H. Kim, T. Ikeda, H. S. Park, H. J. Kim, M. S. Hyun, K. Kano, K. Takagi and H. Tatsumi, *Biotechnol. Tech.*, 1999, **13**, 475–478.
2 D. R. Bond, D. E. Holmes, L. M. Tender and D. R. Lovley, *Science*, 2002, **295**, 483–485.
3 L. M. Tender, C. E. Reimers, H. A. Stecher, D. E. Holmes, D. R. Bond, D. A. Lowy, K. Pilobello, S. J. Fertig and D. R. Lovley, *Nat. Biotechnol.*, 2002, **20**, 821–825.
4 Y. Z. Fan, E. Sharbrough and H. Liu, *Environ. Sci. Technol.*, 2008, **42**, 8101–8107.
5 B. E. Logan, *Nat. Rev. Microbiol.*, 2009, **7**, 375–381.
6 M. H. Osman, A. A. Shah and F. C. Walsh, *Biosens. Bioelectron.*, 2010, **26**, 953–963.

7 A. P. Borole, G. Reguera, B. Ringeisen, Z. W. Wang, Y. J. Feng and B. H. Kim, *Energy Environ. Sci.*, 2011, **4**, 4813–4834.
8 J. C. Wei, P. Liang and X. Huang, *Bioresour. Technol.*, 2011, **102**, 9335–9344.
9 Y. Qiao, S.-J. Bao and C. M. Li, *Energy Environ. Sci.*, 2010, **3**, 544–553.
10 B. E. Logan, B. Hamelers, R. A. Rozendal, U. Schrorder, J. Keller, S. Freguia, P. Aelterman, W. Verstraete and K. Rabaey, *Environ. Sci. Technol.*, 2006, **40**, 5181–5192.
11 E. S. Friedman, M. A. Rosenbaum, A. W. Lee, D. A. Lipson, B. R. Land and L. T. Angenent, *Biosens. Bioelectron.*, 2012, **32**, 309–313.
12 C. I. Torres, R. Krajmalnik-Brown, P. Parameswaran, A. K. Marcus, G. Wanger, Y. A. Gorby and B. E. Rittmann, *Environ. Sci. Technol.*, 2009, **43**, 9519–9524.
13 D. Sun, D. F. Call, P. D. Kiely, A. J. Wang and B. E. Logan, *Biotechnol. Bioeng.*, 2012, **109**, 405–414.
14 D. Pocaznoi, B. Erable, L. Etcheverry, M.-L. Delia and A. Bergel, *Bioresour. Technol.*, 2012, **114**, 334–341.
15 Y. Liu, F. Harnisch, K. Fricke, R. Sietmann and U. Schroder, *Biosens. Bioelectron.*, 2008, **24**, 1006–1011.
16 O. Nercessian, S. Parot, M.-L. Délia, A. Bergel and W. Achouak, *PLoS One*, 2012, **7**, e34216.
17 H. Yi, K. P. Nevin, B.-C. Kim, A. E. Franks, A. Klimes, L. M. Tender and D. R. Lovley, *Biosens. Bioelectron.*, 2009, **24**, 3498–3503.
18 G. He, Y. Gu, S. He, U. Schröder, S. Chen and H. Hou, *Bioresour. Technol.*, 2011, **102**, 10763–10766.
19 D. Pocaznoi, B. Erable, M.-L. Delia and A. Bergel, *Energy Environ. Sci.*, 2012, **5**, 5287–5296.
20 D. Ntarlagiannis, E. A. Atekwana, E. A. Hill and Y. Gorby, *Geophys. Res. Lett.*, 2007, **34**, L17305.
21 S. Parot, M. L. Delia and A. Bergel, *Bioresour. Technol.*, 2008, **99**, 4809–4816.
22 J. Niessen, F. Harnisch, M. Rosenbaum, U. Schroder and F. Scholz, *Electrochem. Commun.*, 2006, **8**, 869–873.
23 G. T. Kim, M. S. Hyun, I. S. Chang, H. J. Kim, H. S. Park, B. H. Kim, S. D. Kim, J. W. T. Wimpenny and A. J. Weightman, *J. Appl. Microbiol.*, 2005, **99**, 978–987.
24 P. Cristiani, A. Franzetti and G. Bestetti, *Electrochim. Acta*, 2008, **54**, 41–46.
25 S. J. Dunaj, J. J. Vallino, M. E. Hines, M. Gay, C. Kobyljanec and J. N. Rooney-Varga, *Environ. Sci. Technol.*, 2012, **46**, 1914–1922.
26 G. C. Gil, I. S. Chang, B. H. Kim, M. Kim, J. K. Jang, H. S. Park and H. J. Kim, *Biosens. Bioelectron.*, 2003, **18**, 327–334.
27 J. Y. Nam, H. W. Kim, K. H. Lim, H. S. Shin and B. E. Logan, *Biosens. Bioelectron.*, 2010, **25**, 1155–1159.
28 C. I. Torres, A. K. Marcus and B. E. Rittmann, *Biotechnol. Bioeng.*, 2008, **100**, 872–881.
29 P. Aelterman, S. Freguia, J. Keller, W. Verstraete and K. Rabaey, *Appl. Microbiol. Biotechnol.*, 2008, **78**, 409–418.
30 D. A. Finkelstein, L. M. Tender and J. G. Zeikus, *Environ. Sci. Technol.*, 2006, **40**, 6990–6995.
31 H. V. M. Hamelers, A. ter Heijne, N. Stein, R. A. Rozendal and C. J. N. Buisman, *Bioresour. Technol.*, 2011, **102**, 381–387.
32 E. Marsili, J. B. Rollefson, D. B. Baron, R. M. Hozalski and D. R. Bond, *Appl. Environ. Microbiol.*, 2008, **74**, 7329–7337.
33 Y. Sharma and B. K. Li, *Bioresour. Technol.*, 2010, **101**, 1844–1850.
34 B. E. Logan and J. M. Regan, *Trends Microbiol.*, 2006, **14**, 512–518.
35 H. Liu, S. A. Cheng and B. E. Logan, *Environ. Sci. Technol.*, 2005, **39**, 658–662.
36 S. M. Strycharz, A. P. Malanoski, R. M. Snider, H. Yi, D. R. Lovley and L. M. Tender, *Energy Environ. Sci.*, 2011, **4**, 896–913.
37 K. Fricke, F. Harnisch and U. Schroder, *Energy Environ. Sci.*, 2008, **1**, 144–147.
38 E. Marsili, J. Sun and D. R. Bond, *Electroanalysis*, 2010, **22**, 865–874.
39 Y. Z. Fan, H. Q. Hu and H. Liu, *Environ. Sci. Technol.*, 2007, **41**, 8154–8158.
40 B. E. Logan, *Microbial fuel cells*, John Wiley & Sons, 2008, vol. 1.
41 K.-J. C. Kim, M.-J. Choi and W. Verstraete, *Environ. Eng. Res.*, 2008, **13**, 51–65.
42 J. K. Jang, T. H. Pham, I. S. Chang, K. H. Kang, H. Moon, K. S. Cho and B. H. Kim, *Process Biochem.*, 2004, **39**, 1007–1012.
43 H. Liu, S. A. Cheng and B. E. Logan, *Environ. Sci. Technol.*, 2005, **39**, 5488–5493.
44 J. Winfield, I. Ieropoulos, J. Greenman and J. Dennis, *Bioelectrochemistry*, 2011, **81**, 22–27.
45 V. J. Watson and B. E. Logan, *Electrochem. Commun.*, 2011, **13**, 54–56.
46 C. I. Torres, A. K. Marcus, P. Parameswaran and B. E. Rittmann, *Environ. Sci. Technol.*, 2008, **42**, 6593–6597.
47 K. P. Nevin, P. Zhang, A. E. Franks, T. L. Woodard and D. R. Lovley, *J. Power Sources*, 2011, **196**, 7514–7518.
48 H. Rismani-Yazdi, S. M. Carver, A. D. Christy and I. H. Tuovinen, *J. Power Sources*, 2008, **180**, 683–694.
49 Y. Zhao, K. Watanabe, R. Nakamura, S. Mori, S. Mori, H. Liu, K. Ishii and K. Hashimoto, *Chem.–Eur. J.*, 2010, **16**, 4982–4985.
50 B. Logan, S. Cheng, V. Watson and G. Estadt, *Environ. Sci. Technol.*, 2007, **41**, 3341–3346.
51 F. Zhao, N. Rahunen, J. R. Varcoe, A. Chandra, C. Avignone-Rossa, A. E. Thumser and R. C. T. Slade, *Environ. Sci. Technol.*, 2008, **42**, 4971–4976.
52 A. Dewan, H. Beyenal and Z. Lewandowski, *Environ. Sci. Technol.*, 2008, **42**, 7643–7648.
53 D. Xing, Y. Zuo, S. Cheng, J. M. Regan and B. E. Logan, *Environ. Sci. Technol.*, 2008, **42**, 4146–4151.
54 K. P. Nevin, H. Richter, S. F. Covalla, J. P. Johnson, T. L. Woodard, A. L. Orloff, H. Jia, M. Zhang and D. R. Lovley, *Environ. Microbiol.*, 2008, **10**, 2505–2514.